



ARTICLE OPEN



Immobilization of silver nanoparticles on cellulose nanofibrils incorporated into nanofiltration membrane for enhanced desalination performance

Ming He^{1,2}[✉], Wei-Dong Li^{1,2}, Jia-Chuan Chen¹, Zhi-Guo Zhang¹¹, Xiao-Fa Wang¹ and Gui-Hua Yang¹[✉]

Nanofiltration (NF) membranes circumventing global water scarcity with excellent separation and antibacterial performances are highly desirable for efficient water treatment but remain a great challenge. Herein, a nanofiltration membrane was fabricated by in situ immobilizing silver nanoparticles (AgNPs) on sulfated cellulose nanofibril incorporated during interfacial polymerization. AgNPs were confirmed to be uniformly distributed and in situ grown on sulfated cellulose nanofibril (SCNF) due to its abundant sulfate and hydroxyl groups by mixing them with anhydrous piperazine solution as inorganic phase and homophenyl chloride n-hexane solution as the organic phase on the surface of a polyethersulfone microporous membrane. The attributes of SCNF, excellent hydrophilicity, and highly negative charges enhanced both the rejection and water permeability. As the SCNF charge increased, the roughness of SCNF increased and the contact angle decreased, and the maximum values were 203 nm and 17.67°, respectively. Among all the composite NF membranes, H-SCNF/Ag-0.01 had better rejection of Na₂SO₄ and NaCl, with a maximum rejection of 97.11% and 32.55%, respectively. Meanwhile, it also maintained high water permeability. Antibacterial experiments indicated that the composite NF membrane had effective inhibition against *Escherichia coli* and exhibited an expected slow-release capability of Ag⁺, which made it have long-term antibacterial properties. It was estimated that the antibacterial effect could last for 90 days. This work demonstrated that AgNPs in situ immobilization on SCNF could be used as promising nanofillers for designing advanced functional NF membranes.

npj Clean Water (2022)5:64; <https://doi.org/10.1038/s41545-022-00217-7>

INTRODUCTION

A nanofiltration (NF) membrane is a pressure-driven separation membrane between reverse osmosis membrane (RO) and ultrafiltration membrane (UF), and its pore size is in the range of 0.2–2 nm¹. It is mainly used for the desalination of salt water, groundwater, and surface water. The most commonly used method for preparing NF is interfacial polymerization (IP)². Polymerization of Piperazine (PIP) aqueous solution and homobenzoyl chloride (TMC) of organic solvent on porous supports are used to prepare NF, which are usually divided into two layers: interface selection layer and supporting bottom membrane³. Water permeability and rejection are essential properties of NF. However, due to the attachment and multiplication of bacteria, the surface of the composite NF membrane is easy to form biofilm⁴. The generated bacterial biofilm leads to the increase of hydraulic resistance and concentration polarization effect of osmotic flow, which reduces the water permeability and rejection rate of the composite NF membrane, and increases the energy loss and operating cost of the composite NF membrane⁵. To reduce biological contamination, researchers usually add disinfectants to water or carry out physical and chemical pretreatment, disinfection, or oxidation of water to inactivate bacteria. But these fungicides can only kill the plankton in the water and have little killing activity on the bacteria and the biofilm generated on the composite NF membrane, and the composite NF membrane will degrade when it comes into contact with chlorine and other chemical oxidants^{6,7}. Other disinfection methods, such as ultraviolet disinfection, its membrane bacteria have a small fire

extinguishing performance. The non-oxidizing disinfectant 2, 2-dibromo-3-nitropropanamide (DBNPA), which requires replenishment after a period of operation, is costly and generates a large waste stream^{8,9}.

In recent years, the introduction of nanoparticles into composite NF membranes to reduce biological contamination has become more and more popular. Commonly used nanoparticles are silver, copper, titanium oxide, and so on^{10–12}. Among all nanoparticles, silver nanoparticles (AgNPs) have the advantages of broad-spectrum antibacterial activity, no bacterial resistance, and low toxicity to mammalian cells, which is recognized as a safe and effective antimicrobial agent¹³. AgNPs can mainly inhibit the growth of microorganisms in three ways. In a first way, AgNPs release Ag⁺, which interacts with enzymes or disulfide or thiol groups of DNA to generate reactive oxygen species or interrupt DNA replication, thus disrupting metabolic processes and leading to bacterial cell damage or even deaths. The second way is that AgNPs attach to the membrane surface and destroy the stability and plasma membrane potential of the outer membrane, thus disrupting the normal function of the membrane. A third way is that small AgNPs can penetrate the cell membrane and enter the bacteria, interacting with compounds containing sulfur or phosphorus, causing further damage to the bacteria^{14,15}. The commonly used methods of adding AgNPs into composite NF membranes include physical bonding, chemical bonding, and layer-by-layer technology¹⁶. However, AgNPs tend to aggregate in the polymer matrix, which dramatically weakens their antibacterial performance. To improve its dispersibility, many researchers have fixed AgNPs on the carrier.

¹State Key Laboratory of Biobased Material and Green Papermaking, Qilu University of Technology, Shandong Academy of Sciences, Jinan 250353, China. ²These authors contributed equally: Ming He, Wei-Dong Li. ✉email: heming8916@qlu.edu.cn; ygh@qlu.edu.cn

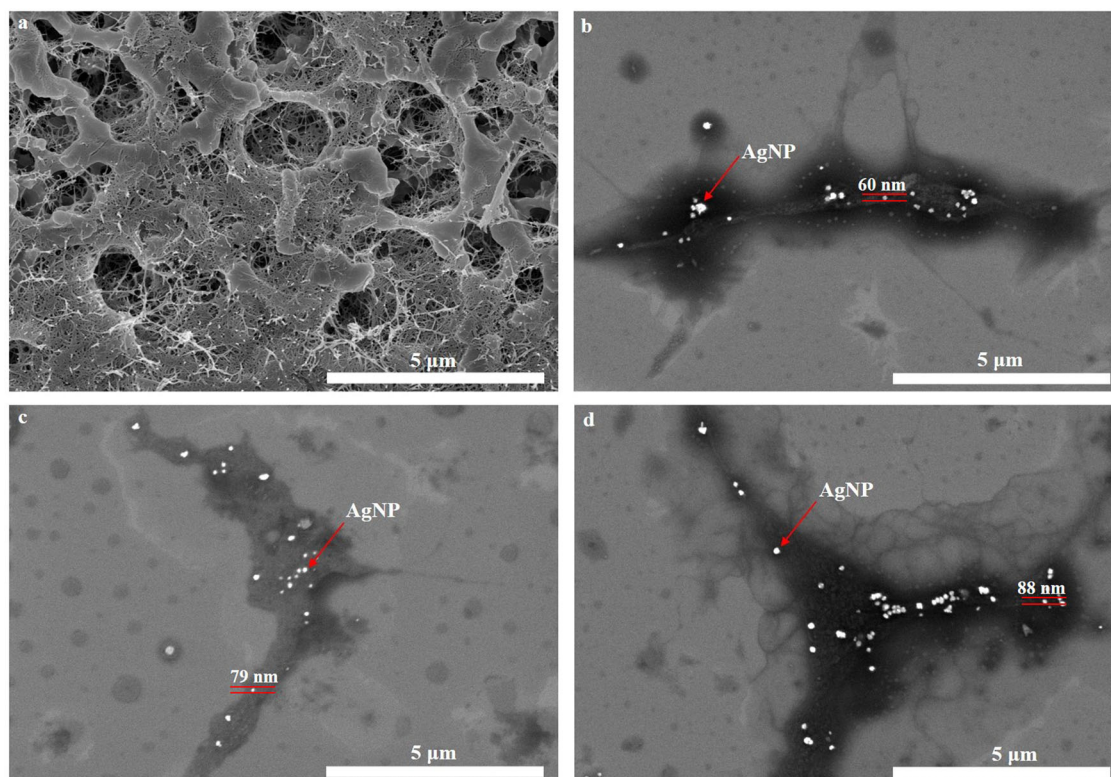


Fig. 1 SEM images of CNF and CNF/Ag nanocomposites. SEM images (scale bar: 5 μm) of **a** L-SCNF, **b** L-SCNF/Ag, **c** M-SCNF/Ag and **d** H-SCNF/Ag.

Nanocellulose as the carrier of AgNPs has attracted the attention of many researchers due to its large specific surface area, environmental friendliness, wide source, and ease of chemical modification¹⁷. Liu et al prepared carboxylated cellulose nanocrystal (CNC) and AgNPs and used them as bi-functional nanofillers to improve the mechanical properties and antibacterial properties of waterborne polyurethane (WPU)¹⁸. Compared with unmodified cellulose, chemically modified cellulose provides more loading sites for AgNPs¹⁹. Sulfated cellulose nanofibril (SCNF) is a kind of nanocellulose with the sulfated group. Due to its good biocompatibility, biodegradability, and abundant sulfate groups and hydroxyl groups, SCNF can be used as a carrier of Ag ions, which can be fixed on SCNF for uniform in situ growth and distribution. This method can effectively reduce the aggregation of AgNPs and improve the dispersion of AgNPs, and promote their full play of antibacterial effect. Furthermore, adding SCNF into the NF membrane can effectively improve the separation performance of the NF membrane due to its hydrophilicity, thus increasing the service life of the NF membrane²⁰. However, few works have been focused on the utilization of SCNF as the carrier of AgNPs in NF membranes so far.

Inspired by these advantages, in this study, SCNFs with different charge amounts were used as the carrier to compound it with Ag, and Ag was grown in situ and distributed uniformly on their surface. The prepared SCNF/Ag complex was mixed with anhydrous piperazine aqueous solution as the inorganic phase. A composite NF membrane loaded with Ag was prepared by IP with an n-hexane solution of homophenyl chloride as the organic phase on the surface of the polyethersulfone microporous membrane. The prepared SCNF/Ag composite was analyzed by scanning electron microscope (SEM), X-ray diffraction photoelectron spectroscopy (XPS), and X-ray diffractometer (XRD). The composite NF membrane was characterized by an infrared spectrometer, XPS, SEM, atomic force microscope (AFM), contact angle measuring instrument, laboratory self-made separation, and

detection device, and atomic spectrophotometer. The antibacterial performance of the NF membrane was tested by a bacteriostatic zone experiment.

RESULTS AND DISCUSSION

Characterization of CNF and CNF/Ag nanocomposites

The surface morphology of SCNF and SCNF/Ag nanocomposites were characterized by SEM. As shown in Fig. 1a, SCNF was filamentous with a high aspect ratio. The fibers were intertwined to form a network structure. Since the SCNF surface had a large number of negatively charged sulfate groups and rich hydroxyl groups, Ag^+ was well fixed by electrostatic adsorption and ion-dipole interaction²¹. Figure 1b–d was SEM images of SCNF/Ag nanocomposites, which showed AgNPs were in situ immobilized on SCNF. It is known that the distribution of AgNPs on the membrane surface was essential that continuous AgNPs precipitation would lead to membrane surface blockage and reduce membrane permeability²². It could be seen from the figures that AgNPs were discretely distributed instead of aggregation, and AgNPs had uniform dispersion and little aggregation on SCNF.

XRD spectra of SCNF and SCNF/Ag nanocomposite were shown in Supplementary Fig. 1a. As shown in Supplementary Fig. 1a, For SCNF, the diffraction peaks at 14.94, 16.56, 22.4, and 33.84 are consistent with the (110), (110), (200), and (004) planes of typical cellulose, respectively. In addition, new peaks appeared in samples L-SCNF/Ag, M-SCNF/Ag, and H-SCNF/Ag at 38.26°, 44.36°, 64.74°, and 77.46°, corresponding to the diffraction peaks of (111), (200), (220), and (311) planes of AgNPs²³. This indicated that AgNPs were successfully grown in situ on SCNF.

Supplementary Fig. 1b was the XPS spectra of SCNF and SCNF/Ag nanocomposites. All samples had two strong peaks at the binding energies of 286 and 532 eV, belonging to C1s and O1s, respectively. Moreover, samples of L-SCNF/Ag, M-SCNF/Ag, and H-SCNF/Ag showed new peaks at the binding energy of 368 eV,

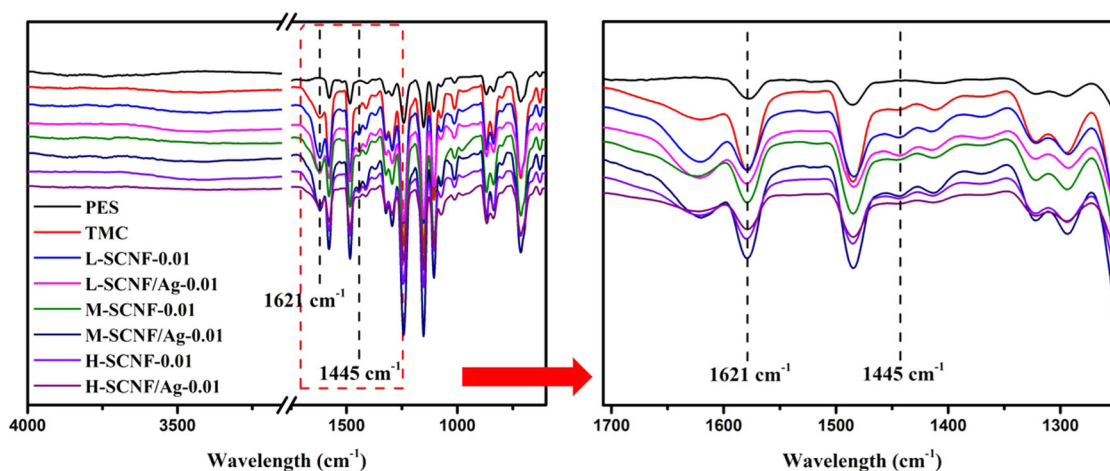


Fig. 2 FTIR spectra of composite NF membrane. FTIR spectra of PES substrate, SCNF composite NF membrane and SCNF/Ag composite NF membrane.

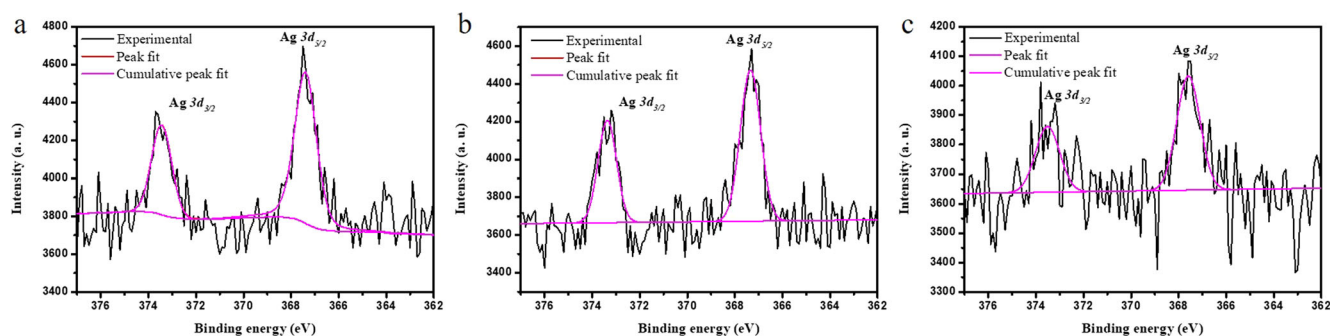


Fig. 3 The Ag 3d XPS spectra of SCNF/Ag composite NF membrane. The Ag 3d XPS spectra of **a** L-SCNF/Ag-0.01, **b** M-SCNF/Ag-0.01 and **c** H-SCNF/Ag-0.01.

which was attributed to the signal peak of Ag 3d. This further proved the existence of Ag in the zero-oxidation state, which provided favorable evidence for the successful in situ growth of AgNPs on SCNF.

Surface chemical structure of composite nanofiltration membrane

FTIR spectra of the PES substrate, SCNF composite NF membrane, and SCNF/Ag composite NF membrane were shown in Fig. 2. As demonstrated in Fig. 2, after IP, two new characteristic peaks appeared in the composite NF membrane at wavelength 1443 and 1621 cm^{-1} , respectively, which were attributed to the stretching vibration of C=O in the -CO-NH-group and the stretching vibration of O-H in the carboxyl group generated by unreactive acyl chloride hydrolysis²⁴. The appearance of these two characteristic peaks indicated that the surface of the membrane had a polyamide structure, indicating the success of IP. The typical cellulose characteristic peaks of SCNF and SCNF/Ag were not detected, which might be due to being covered by the strong peaks of the polyamide layer.

The Ag 3d XPS spectra of L-SCNF/Ag-0.01, M-SCNF/Ag-0.01, and H-SCNF/Ag-0.01 were shown in Fig. 3. As shown in Fig. 3, L-SCNF/Ag-0.01, M-SCNF/Ag-0.01, and H-SCNF/Ag-0.01 all had two strong peaks at 367.4 and 373.5 eV, corresponding to Ag 3d_{5/2} and Ag 3d_{3/2} peaks, respectively. Ag 3d_{5/2} and Ag 3d_{3/2} were typical peaks of AgNPs²⁵. This further proved the successful preparation of AgNPs and their existence on the surface of NF membrane.

Surface characterization of composite nanofiltration membrane

The SEM images of the PES substrate and composite NF membrane were shown in Fig. 4. Figure 4a was the SEM image of the PES substrate. It could be seen from the image that the PES substrate had a smooth surface, and holes were evenly distributed on the surface. Figure 4b–(e) were SEM images of TFC, L-SCNF-0.01, M-SCNF-0.01, and H-SCNF-0.01, respectively, indicating that the surface of the composite NF membrane had a ridge valley structure. Figure 4(f)–(h) were the SEM images of L-SCNF/Ag-0.01, M-SCNF/Ag-0.01, and H-SCNF/Ag-0.01, respectively. The surface of the composite NF membrane seemed to be covered by SCNF/Ag nanocomposites. Small bright features were detected on the surface of the composite NF membrane, which also had a ridge valley structure. This was similar to the Turing nanostructure of polyamide reported by Tan et al.²⁶. The fringe Turing structure was mainly due to the self-inhibition process generated by hydrogen bond interaction between SCNF and excess TMC during IP²⁷. The high permeability site of the Turing structure could improve the water permeability of the NF membrane. Adding the same amount of SCNF into the interface selection layer also had a ridge valley structure, which further proved that the Turing structure was caused by the hydrogen bond interaction between SCNF and excess TMC. With the increase of the charge of SCNF, the Turing structure became more scattered and disordered.

AFM images of the composite NF membrane were shown in Fig. 5. As shown in Fig. 5, the mean square roughness (Rq) of the composite NF membrane increased from 31.3 to 203 nm after adding SCNF or SCNF/Ag composite into the interface selection

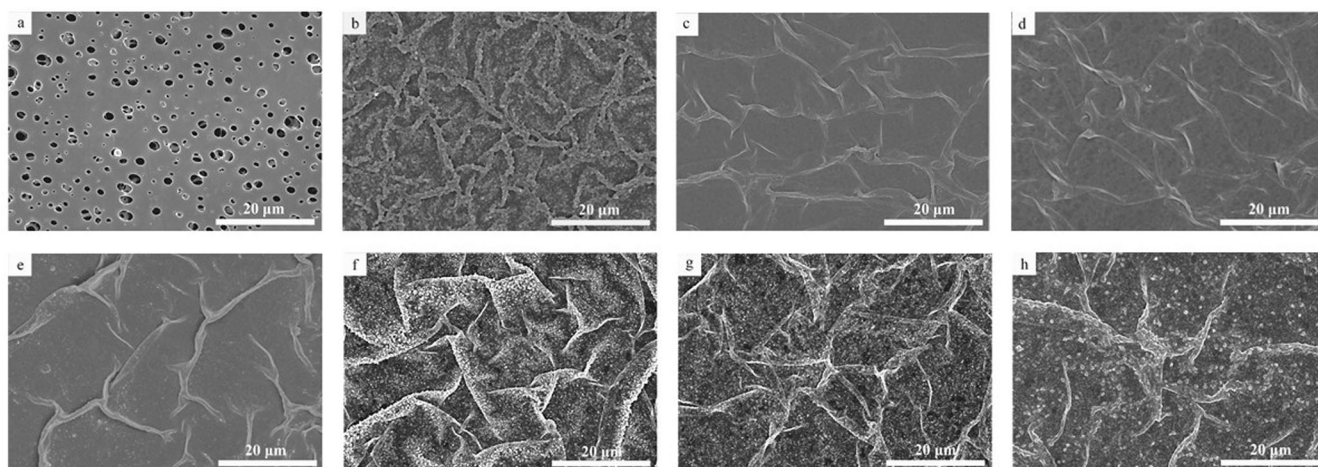


Fig. 4 SEM images of composite NF membrane. SEM images (scale bar: 20 μm) of **a** PES substrate, **b** TFC, **c** L-SCNF-0.01, **d** M-SCNF-0.01, **e** H-SCNF-0.01, **f** L-SCNF/Ag-0.01, **g** M-SCNF/Ag-0.01 and **h** H-SCNF/Ag-0.01.

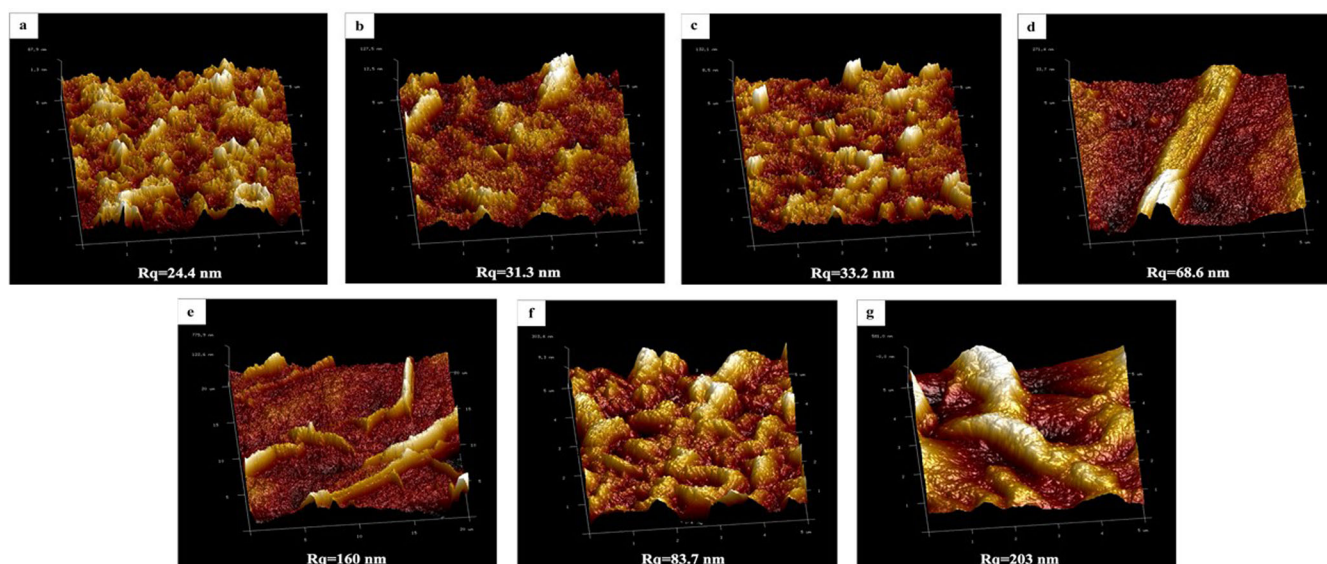


Fig. 5 AFM images of composite NF membrane. AFM images (scale bar: 5 μm) of **a** TFC, **b** L-SCNF-0.01, **c** L-SCNF/Ag-0.01, **d** M-SCNF-0.01, **e** MSCNF/Ag-0.01, **f** H-SCNF-0.01 and **g** H-SCNF/Ag-0.01.

layer. This could be explained by the fact that the hydrophilicity of SCNF and SCNF/Ag composite increased the hydrophilicity of the inorganic phase and reduced the diffusion of PIP from the inorganic to the organic phase, thus increasing the surface roughness of the composite NF membrane²⁸. The viscosity of the inorganic phase increased after the addition of SCNF/Ag composite, further limiting PIP diffusion from the inorganic phase to the organic phase, resulting in a rougher surface. The roughness of the composite NF membrane increased with the increase of the charge of SCNF. This was due to the fact that the increase of charge of SCNF enhanced the hydrophilicity of SCNF and increased the roughness of the composite NF membrane. Noticeably, the results were consistent with SEM results.

Contact angle of composite nanofiltration membrane

The hydrophilicity of the membrane was assessed by measuring the water contact angle, as it was an important film property that could affect the performance of the membrane. The contact angle of the composite NF membrane was shown in Fig. 6. As shown in Fig. 6, after SCNF and SCNF/Ag composite were added into the interface

selection layer of the composite NF membrane, the surface contact angle of the composite NF membrane decreased. The minimum contact angle was 17.67° of H-SCNF/Ag-0.01, which was 30.92% lower than that of TFC, indicating that the hydrophilicity of the composite NF membrane was enhanced. As shown in Fig. 6, the contact angle of the NF membrane decreased with the increase of SCNF charge. This was mainly due to the hydrophilicity of SCNF itself, and the hydrophilicity of SCNF increased with the increase of charge. The water permeability of the NF membrane was affected by the contact angle. The contact angle decreased, hydrophilicity increased, and water permeability increased. In addition, it could be seen in Fig. 6 that the contact angle of the membrane with SCNF/Ag composite was smaller than that of the membrane with SCNF. This experimental result was consistent with the previous studies^{29,30}. This indicated that adding SCNF/Ag composite to the polyamide layer of the composite NF membrane could improve the hydrophilicity of the composite NF membrane, which was attributed to the presence of a hydrophilic silver oxide layer on the surface of AgNPs³¹. More hydrophilic surfaces could both improve water permeability by increasing the membrane's water solubility and resistance to biological contamination by reducing bacterial adhesion³².

Separation performance of composite nanofiltration membrane

The separation performance of the composite NF membrane was shown in Fig. 7. Figure 7a was the rejection and water permeability of composite NF membrane for Na_2SO_4 . As shown in Fig. 7a, compared with TFC, the rejection of the composite NF membrane increased with a maximum increase of 7.36% after the addition of SCNF and SCNF/Ag composite. The rejection of the composite NF membrane increased from 92.65% to 97.11% with the increase of the charge of SCNF. The order of Na_2SO_4 rejection of composite NF membranes was as follows: H-SCNF/Ag-0.01 > H-SCNF-0.01 > M-SCNF/Ag-0.01 > M-SCNF-0.01 > L-SCNF/Ag-0.01 > L-SCNF-0.01. Meanwhile, the water permeability of the composite NF membrane increased from 108.28 to 351.38 $\text{L}/\text{m}^2/\text{h}$. This was due to the Turing structure of the composite NF membrane, which increased the contact area between the membrane surface and water and broke the upper limit of the permeation-selection equilibrium of the composite NF membrane, thus increasing both the rejection and water permeability of the composite NF membrane²⁶. In addition, compared with SCNF, the addition of SCNF/Ag composite could improve the rejection and water permeability of the composite NF membrane. This was because the composite NF membrane with SCNF/Ag composite had a more hydrophilic surface and a rougher surface than the composite NF membrane with SCNF. According to the previous studies, the addition of SCNF/Ag composite was conducive to improving the cross-linking reaction in the IP process and effectively improving the rejection rate of composite NF

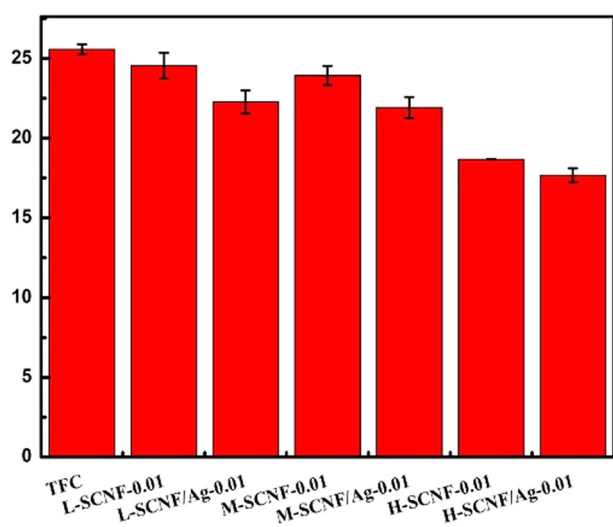
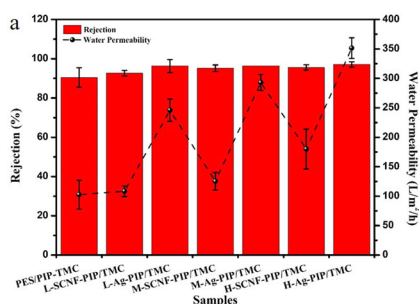


Fig. 6 Contact angle of composite nanofiltration membrane. Error bars represent standard deviations using at least two measurements from two different samples.



membranes²⁷. Figure 7b was the rejection and water permeability of composite NF membrane for NaCl. With the increased charge of SCNF, the rejection and water permeability of the composite NF membrane increased. H-Ag-PIP/TMC had the highest retention rate and water permeability, which were 32.55% and 206.63 $\text{L}/\text{m}^2/\text{h}$, respectively. Figure 7 showed that the rejection of the composite NF membrane for Na_2SO_4 was higher than that for NaCl, which was because the hydration radius of the divalent ion was larger than that of the monovalent ion, so it was easier for the monovalent ion to pass through the interface selection layer of the composite NF membrane. Among seven composite NF membranes, H-SCNF/Ag-0.01 showed excellent desalination performance.

Antibacterial performance of composite nanofiltration membrane

Figure 8 showed the antibacterial experimental results of the H-SCNF/Ag-0.01 composite NF membrane with a diameter of 8 mm. As shown in Fig. 8, TFC and H-SCNF-0.01 composite NF membrane did not affect the growth of *Escherichia coli*, while H-SCNF/Ag-0.01 composite NF membrane showed a clear AGAR surface with no bacterial growth, and an inhibition zone (0.35 mm) was observed around it. This was consistent with previous studies showing that AgNPs had an antibacterial effect, with inhibition zones occurring around substrates containing AgNPs³³. Figure. S2 showed the antibacterial test results of TFC, L-SCNF-0.01, L-SCNF/Ag-0.01, M-SCNF-0.01, and M-SCNF/Ag-0.01. As shown in Fig. S2, inhibition zones were observed around L-SCNF/Ag-0.01 and M-SCNF/Ag-0.01 composite nanofiltration membranes, which were similar to H-SCNF/Ag-0.01 composite nanofiltration membranes. After removing the membrane samples, bacterial growth was observed on the AGAR surface of L-SCNF-0.01 and M-SCNF-0.01 membranes, while no bacterial growth was observed on the AGAR surface of H-SCNF/Ag-0.01 membranes. These results indicated that L-SCNF/Ag-0.01 and M-SCNF/Ag-0.01 composite nanofiltration membranes had an inhibitory effect on *E. coli*. AgNPs could mainly inhibit the growth of microorganisms in three ways. The first way was that AgNPs releases Ag^+ and interacted with the disulfide or mercaptan groups of enzymes or DNA to generate reactive oxygen species or interrupt replication, thus disrupting metabolic processes and leading to bacterial cell damage or even death. The second way was that AgNPs attach to the membrane surface and destroy the stability and plasma membrane potential of the outer membrane, thus disrupting the normal function of the membrane. The third way was that AgNPs with small particle size could penetrate the cell membrane into the bacteria and interact with sulfur or phosphorus-containing compounds, causing further damage to the bacteria³⁴. This indicated that TFC membrane surface was prone to membrane biological contamination, and adding AgNPs in the NF membrane could inhibit biological contamination.

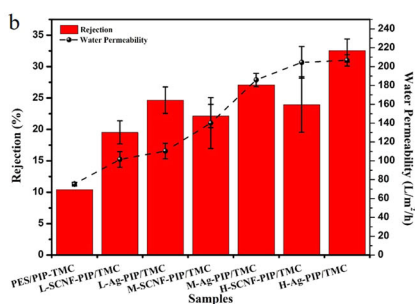


Fig. 7 Rejection and water permeability of composite NF membrane for Na_2SO_4 and NaCl. **a** Rejection and water permeability of composite NF membrane for Na_2SO_4 , **b** Rejection and water permeability of composite NF membrane for NaCl. Error bars represent standard deviations using at least two measurements from two different samples.

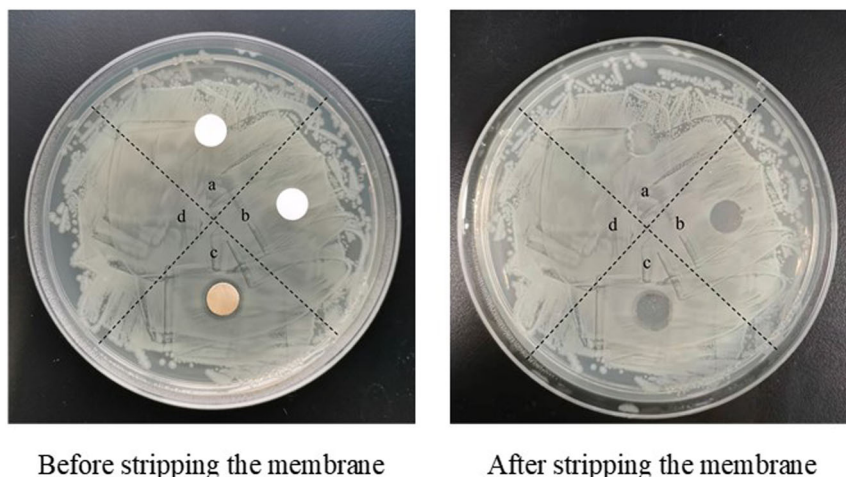


Fig. 8 Bacteriostatic zone experiment, the diameter of the membrane was 8 mm, and the membrane was removed from the nutrient AGAR after 24 h culture. a TFC, b H-SCNF-0.01, c H-SCNF/Ag-0.01 and d Blank bacteriostatic zone experiment, the diameter of the membrane was 8 mm, and the membrane was removed from the nutrient AGAR after 24 h culture.

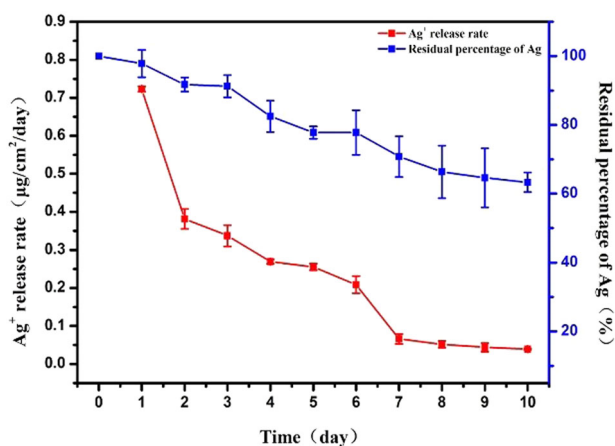


Fig. 9 Ag⁺ release rate and residual percentage of H-SCNF/Ag-0.01. Error bars represent standard deviations using at least two measurements from two different samples.

Stability analysis of silver in nanofiltration membrane

To evaluate the duration of the antibacterial effect of the composite NF membrane, the stability of silver in the composite NF membrane was measured over a period of time. Figure 9 showed the silver ion release rate and residual percentage of silver in the prepared composite NF membrane within 10 days. As shown in Fig. 9, the release rate of composite NF membrane was 0.72 $\mu\text{g}/\text{cm}^2/\text{day}$ on the first day, 0.38 $\mu\text{g}/\text{cm}^2/\text{day}$ on the second day, and 0.34 $\mu\text{g}/\text{cm}^2/\text{day}$ on the third day. The silver release rate in the first 3 days was still at a high level. However, after the third day, the release rate of silver ions reached a stable level. This was mainly because the initial release process of silver ions was generally controlled by the diffusion of water on the substrate surface. For the film surface with AgNPs, silver ions were easy to diffuse on the surface, leading to the rapid diffusion of silver ions in the initial stage³⁵. SCNF had a large specific surface area and was a suitable carrier for stabilizing AgNPs, which could effectively prevent Ag leaching from SCNF/Ag composite. In addition, SCNF showed excellent compatibility in the polymer matrix due to its large specific surface area, which also contributed to the stability of AgNPs in polyamide layers³⁶. This trend of high initial rates followed by a sudden decline was consistent with the results obtained by other researchers³⁷. At a stable release period after 3 days, the residual percentage of silver decreased linearly with time,

and the average release rate was 0.04 $\mu\text{g}/\text{cm}^2/\text{day}$. Based on the average release rate and residual percentage of silver, the antibacterial effect of silver was expected to last for 90 days, which was similar to other expected duration reported in the literature^{38,39}.

In this work, AgNPs were in situ immobilized on SCNF, and the composite was incorporated into the selective layer as the inorganic phase via IP to fabricate an NF membrane. Benefit from excellent hydrophilicity and highly negative charges of SCNF, the water permeability of the NF membrane could be improved by the high permeability site of the Turing structure formed by SCNF and excess TMC. Furthermore, SCNF had a large specific surface area and was an ideal carrier for dispersing and stabilizing AgNPs, which could effectively prevent Ag leaching from SCNF/Ag composite. In addition, the influence of SCNF with different charges on composite NF membranes was investigated. With the increase of SCNF charge, the surface roughness of the composite NF membrane increased, and its maximum value was 203 nm, while the water contact angle decreased, and its minimum value was 17.67°, which was mainly due to the hydrophilicity and viscosity of the SCNF/Ag composite. After SCNF/Ag composite addition, the interception rate and water permeability of the composite NF membrane to salt solution increased. Among all the membranes, H-SCNF/Ag-0.01 NF membranes had the highest rejection rates for Na_2SO_4 solution and NaCl solution, which were 97.11% and 32.55%, respectively. Moreover, H-SCNF/Ag-0.01 NF membranes had higher rejection rates for divalent salt ions than for monovalent salt ions. Due to the antibacterial action of AgNPs, H-SCNF/Ag-0.01 composite NF membrane had good silver stability, and the antibacterial effect of silver could be estimated to last for 90 days. In summary, with excellent water dispersion, large specific surface area, and strong negative charge, SCNF could be used as nanocarriers of AgNPs in the selective layer to achieve an NF membrane with good separation and antibacterial properties.

METHODS

Materials and chemicals

Bleached kraft poplar pulp board (with 85.05% cellulose, 14.55% hemicellulose, and 0.4% lignin) was purchased from Huatai Paper Co., Ltd in Dongying, Shandong Province, China. It was disintegrated in water, filtered, and dried in an oven at 60 °C for 24 h. Glycerol ($\geq 99\%$) and silver nitrate (AgNO_3 , $\geq 99.8\%$) were purchased from Sinopharm Chemical Reagent Co., Ltd. (Shanghai, China). The polyethersulfone (PES) microfiltration membrane (0.22 μm) was purchased from Tianjin Jinteng Experimental Co., Ltd (China). Sulfamic acid (99.5%), piperazine (PIP, $>99\%$), trimesoyl chloride (TMC, 99%), n-hexane

(97%), ammonium hydroxide solution (H_5NO , 25–28%), glucose ($\text{C}_6\text{H}_{12}\text{O}_6$, the molecular weight is 180.16, $\geq 99.5\%$), sodium sulfate (Na_2SO_4) and sodium chloride (NaCl) were all obtained from Shanghai Macklin Biochemical Co., Ltd. (Shanghai, China) and used as received without further purification. Nitric acid (HNO_3) was bought from Laiyang Economic and Technological Development Zone Fine Chemical Plant (Shandong, China). Deionized water (25 °C) was employed in all experiments.

Preparation of SCNF and SCNF/Ag nanocomposites

SCNFs with different surface charges were prepared according to the method reported by Li et al.⁴⁰. The SCNF with low, medium, and high charges were named L-SCNF, M-SCNF, and H-SCNF, respectively. The prepared SCNF with different surface charges was configured as a suspension of 12.5 g/L and stirred magnetically at 70 °C for 30 min. Then add ammonia drop by drop into AgNO_3 solution and gently stir until the brown precipitate disappears to prepare 0.5 mol/L silver ammonia solution ($\text{Ag}(\text{NH}_3)_2\text{OH}$). Evenly transferred the prepared silver ammonia solution to the well-dispersed SCNF solution and stirred vigorously for 20 min to obtain the mixed solution. Finally, 5.98 g glucose solution was added to the above-prepared mixed solution and stirred at 70 °C for 3.5 h to prepare SCNF/Ag nanocomposites. The SCNF/Ag nanocomposite aqueous solution was centrifuged three times to clean the SCNF/Ag nanocomposite thoroughly. The SCNF/Ag nanocomposite powder was prepared after being placed in a vacuum drying oven at 70 °C for 24 h. SCNF prepared by low, medium, and high charge and Ag nanocomposites were named L-SCNF/Ag, M-SCNF/Ag, and H-SCNF/Ag.

Characterization of SCNF and SCNF/Ag nanocomposites

The surface morphology of SCNF and SCNF/Ag nanocomposites was characterized by scanning electron microscopy (SEM, Hitachi Regulus® Regulus 8220, Japan). The chemical composite of SCNF and SCNF/Ag nanocomposites were examined with X-ray photoelectron spectroscopy (XPS, ESCALAB Xi+, Thermo Fisher Scientific, UK). The wide-angle X-ray diffractometry (WAXD, Bruker D8 ADVANC, Germany) was used to characterize the crystal structure of SCNF and SCNF/Ag nanocomposites.

Preparation of composite nanofiltration membrane

SCNF/Ag nanocomposites with SCNFs with different charges and SCNF were prepared into 0.01 wt% mixed solution with ionic water and sonicated for 20 min, respectively. Then, 2.0 wt% PIP aqueous solution was added to SCNF/Ag suspension and SCNF

suspension, respectively. The inorganic phase was prepared after sonication of the above solution for 20 min. Immerse the PES support bottom layer in deionized water for at least 20 min to saturate the membrane, then completely remove the surface water on the PES support bottom layer with a rubber roller, and stick the PES support bottom layer to the surface of a glass plate. Pour the inorganic phase on the PES support bottom layer and soaked it for 2 min. After the time was completed, removed the excess solution on the bottom layer surface and air dry the membrane at room temperature for 10 min until there were no water droplets on the surface of the membrane. Finally, the PES supporting bottom layer was immersed in 0.5 wt% TMC n-hexane solution for 1 min. After the time was completed, the PES supporting bottom film was cured in an oven at 50 °C for 10 min for further polymerization. After the IP process, the L-SCNF-0.01, M-SCNF-0.01, H-SCNF-0.01, L-SCNF/Ag-0.01, M-SCNF/Ag-0.01, and H-SCNF/Ag-0.01 NF membranes were prepared, respectively. TFC NF membrane was prepared by the same IP method only with 2.0 wt% PIP aqueous solution as an inorganic phase. The conditions of membrane preparation in this experiment were shown in Supplementary Table 1. The preparation process was shown in Fig. 10.

Characterization of composite nanofiltration membrane

The chemical structure of the composite NF membrane was studied using Fourier transform infrared (FTIR, Bruker ALPHA, Germany). The spectra and the resolution were from 4000 to 600 cm^{-1} and 2 cm^{-1} , respectively. X-ray photoelectron spectroscopy (XPS, ESCALAB Xi+, Thermo Fisher Scientific, UK) was equipped to analyze the surface elemental of the composite NF membrane. The surface topography of the composite NF membrane was analyzed by SEM (Hitachi Regulus® Regulus 8220, Japan) at 5 kV. Samples were freeze-dried before testing and coated with gold with a sputter coater. The surface roughness of the composite NF membrane was characterized by atomic force microscopy (AFM, Bruker Multimode 8, Germany). All NF membrane samples were freeze-dried before testing. Contact angle goniometer (LSA 100, LAUDA Scientific, Germany) measurements for hydrophilicity of composite NF membrane.

Separation performance

The separation performance of the as-prepared composite NF membrane was evaluated with a lab-scale cross-flow filtration system. The effective area of the membrane was 12.56 cm^2 . The transmembrane pressure was fixed at 2 bar and the concentration

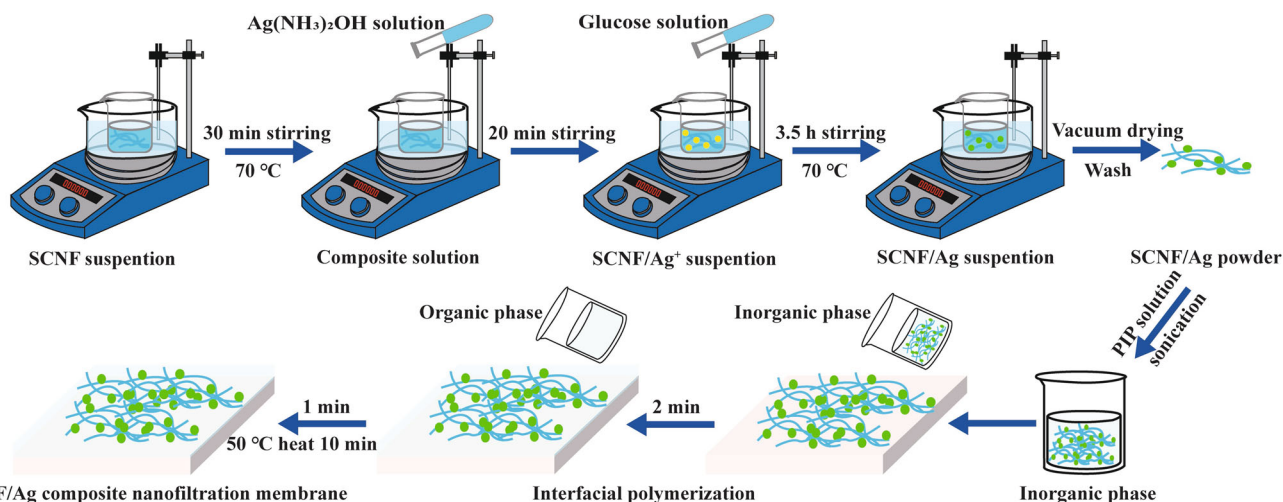


Fig. 10 Preparation process of SCNF/Ag nanocomposites and SCNF/Ag composite NF membranes.

of the feed salt solution was 1000 ppm. To reach stable membrane performance before testing, the composite NF membrane was pre-pressurized at 4 bar for 2 h at room temperature with deionized water. The filtrate solution was collected after running for 30 min under 2 bar. The concentration of filtrate was detected by a conductivity meter (Rex DDS-307A, China). The permeate flux (F , $L m^{-2} h^{-1}$) was calculated based on Eq. (1).

$$F = \frac{V}{A \times t} \quad (1)$$

Where V was the volume of the water permeate (L), A was the effective area of the tested membrane (m^2), and t was the time interval between filtrate collection (h).

The salt rejection ration (R , %) was calculated based on Eq. (2).

$$R = \left(1 - \frac{C_p}{C_f}\right) \times 100\% \quad (2)$$

Where C_p was the concentration of filtered solution and C_f was the concentration of feed solution.

Antibacterial test

E. coli (ECC 133264) was used as model bacteria to detect the antibacterial activity of the composite NF membrane. Before testing, the sample was sterilized under a UV lamp for one hour. The antibacterial activity of the composite NF membrane was evaluated by the AGAR plate bacteriostatic zone method. First, *E. coli* was inoculated into an LB broth liquid medium and incubated at 37 °C for one night. Then, the cultured bacterial suspension was centrifuged at a speed of 2700 r/min for 10 min. After the supernatant was poured out, LB broth liquid medium was used for dilution to obtain the bacterial suspension. The resulting bacterial suspension was diluted to approximately 105 bacterial formation units (CFU)/mL prior to use. Take 50 mL of the above diluted bacterial suspension on the nutrient AGAR plate, and smear it evenly on the nutrient AGAR plate with a triangular coating stick. Then, the composite NF membrane samples with diameters of 8 mm were placed on the nutritional AGAR plate. When placed, the polyamide layer of the composite NF membrane was in contact with the nutritional AGAR surface. Finally, the nutrient AGAR plate was placed in a constant temperature incubator at 37 °C for 24 h, and the bacterial formation under the composite NF membrane was detected.

Release test of Ag ion in composite nanofiltration membrane

The composite NF membrane was cut to a size of 5 cm², immersed in a beaker containing 20 mL of deionized water, and stirred at 50 rpm at room temperature. The solution was collected every 24 h and replaced with deionized water for 10 consecutive days. The collected solution was acidified with 2.0 wt% HNO₃ solution, and the Ag content was analyzed by inductively coupled plasma optical emission spectroscopy (ICP-OES). Then, a 5 cm² composite NF membrane was immersed in 2.0 wt% HNO₃ solution for ultrasonic for 20 min to dissolve all Ag nanoparticles on the membrane surface, and the Ag content was detected by ICP-OES.

Received: 11 August 2022; Accepted: 15 December 2022;

Published online: 24 December 2022

REFERENCES

- Diksha, Y., Sachin, K. & Pravin, I. Nanofiltration (NF) membrane processing in the food industry. *Food Eng. Rev.* **14**, 579–595 (2022).
- Mohammad, A. W. et al. Nanofiltration membranes review: recent advances and future prospects. *Desalination* **356**, 226–254 (2015).
- Li, Y. et al. Preparation of highly selective nanofiltration membranes by moderately increasing pore size and optimizing microstructure of polyamide layer. *J. Membr. Sci.* **643**, 120056 (2022).
- Gómez, J. M. G. & Amils, R. Novel cellular autoaggregative developmentally CRP regulated behaviour generates massively chondrule-like formations over surface of old *Escherichia coli* K-12 macrocolony biofilms. *Nat. Rev. Microbiol.* **8**, 623–633 (2014).
- Matin, A., Khan, Z., Zaidi, S. M. J. & Boyce, M. C. Biofouling in reverse osmosis membranes for seawater desalination: phenomena and prevention. *Desalination* **281**, 1–16 (2011).
- Davies, D. Understanding biofilm resistance to antibacterial agents. *Nat. Rev. Drug Discov.* **2**, 114–122 (2003).
- Perreault, F., Tousley, M. E. & Elimelech, M. Thin-film composite polyamide membranes functionalized with biocidal graphene oxide nanosheets. *Environ. Sci. Technol. Lett.* **1**, 71–76 (2016).
- Kim, D., Jung, S., Sohn, J., Kim, H. & Lee, S. Iodic application for controlling biofouling of SWRO membranes: an overview. *Desalination* **238**, 43–52 (2009).
- Da-Silva-Correa, L. H., Smith, H., Thibodeau, M. C., Welsh, B. & Buckley, H. L. The application of non-oxidizing biocides to prevent biofouling in reverse osmosis polyamide membrane systems: a review. *J. Water Supply* **71**, 261–292 (2022).
- Yang, K. et al. Graphene oxide nanofiltration membranes containing silver nanoparticles: tuning separation efficiency via nanoparticle size. *Nanomaterials* **10**, 454–467 (2020).
- Zareei, F. & Hosseini, S. M. A new type of polyethersulfone based composite nanofiltration membrane decorated by cobalt ferrite-copper oxide nanoparticles with enhanced performance and antifouling property. *Sep. Purif. Technol.* **226**, 48–58 (2019).
- Li, Y. et al. Novel high-flux polyamide/TiO₂ composite nanofiltration membranes on ceramic hollow fibre substrates. *J. Membr. Sci.* **565**, 322–330 (2018).
- Zhang, X., Liu, Z., Shen, W. & Gurunathan, S. Silver nanoparticles: synthesis, characterization, properties, applications, and therapeutic approaches. *Int. J. Mol. Sci.* **17**, 1534–1568 (2016).
- Ashe, S., Nayak, D., Kumari, M. & Nayak, B. Ameliorating effects of green synthesized silver nanoparticles on glycated end product induced reactive oxygen species production and cellular toxicity in osteogenic Saos-2 cells. *ACS Appl. Mater. Interfaces* **8**, 30005–30016 (2016).
- Wang, Y. et al. Antibiotic-loaded, silver core-embedded mesoporous silica nanovehicles as a synergistic antibacterial agent for the treatment of drug-resistant infections. *Biomaterials* **101**, 207–216 (2016).
- Ursino, C. et al. Progress of nanocomposite membranes for water treatment. *Membrane* **8**, 18–58 (2018).
- Zhang, Q., Zhang, L., Wu, W. & Xiao, H. Methods and applications of nanocellulose loaded with inorganic nanomaterials: a review. *Carbohydr. Polym.* **229**, 115454 (2020).
- Liu, H., Song, J., Shang, S., Song, Z. & Wang, D. Cellulose nanocrystal/silver nanoparticle composites as bifunctional nanofillers within waterborne polyurethane. *ACS Appl. Mater. Interfaces* **4**, 2413–2419 (2012).
- Zhang, L., Li, Q., Duan, L. & Liu, R. Preparations and characterisation of a nanosilver-loaded aerogel based on nanocellulose. *Micro Nano Lett.* **15**, 409–414 (2020).
- Li, W. et al. Fabrication of high-performance nanofiltration membranes by using sulfated cellulose nanofibril as the intermediate support layer. *Desalination* **532**, 115741–115752 (2022).
- Grishkewich, N., Mohammed, N., Tang, J. & Tam, K. C. Recent advances in the application of cellulose nanocrystals. *Curr. Opin. Colloid Interface Sci.* **29**, 32–45 (2017).
- Ben-Sasson, M. et al. In situ formation of silver nanoparticles on thin-film composite reverse osmosis membranes for biofouling mitigation. *Water Res.* **62**, 260–270 (2014).
- Xu, C., Chen, W., Gao, H., Xie, X. & Chen, Y. Cellulose nanocrystal/silver (CNC)/thin-film nanocomposite nanofiltration membranes with multifunctional properties. *Env. Sci.* **7**, 803–816 (2020).
- Liu, S. S. et al. Enhancement of desalination performance of thin-film nanocomposite membrane by cellulose nanofibers. *J. Membr. Sci.* **592**, 117363–117386 (2019).
- Wen, P. et al. Preparation and characterization of melamine-formaldehyde/Ag composite microspheres with surface-enhanced Raman scattering and antibacterial activities. *J. Colloid Interface Sci.* **531**, 544–554 (2018).
- Tan, Z., Chen, S., Peng, X., Zhang, L. & Gao, C. Polyamide membranes with nanoscale Turing structures for water purification. *Science* **360**, 518–521 (2018).
- Zhang, R. et al. A novel polyesteramide thin film composite nanofiltration membrane prepared by interfacial polymerization of serinol and trimesoyl chloride (TMC) catalyzed by 4-dimethylaminopyridine (DMAP). *J. Membr. Sci.* **542**, 68–80 (2017).
- Qu, P., Tang, H., Gao, Y., Zhang, L. & Wang, S. Polyethersulfone composite membrane blended with cellulose fibrils. *BioResources* **5**, 2323–2336 (2010).
- Kim, E. S., Hwang, G., El-Din, M. G. & Liu, Y. Development of nanosilver and multiwalled carbon nanotubes thin-film nanocomposite membrane for enhanced water treatment. *J. Membr. Sci.* **394–395**, 37–48 (2012).

30. Yin, J., Yang, Y., Hu, Z. Q. & Deng, B. Attachment of silver nanoparticles (AgNPs) onto thin-film composite (TFC) membranes through covalent bonding to reduce membrane biofouling. *J. Membr. Sci.* **441**, 73–82 (2013).
31. Sawada, I. et al. Development of a hydrophilic polymer membrane containing silver nanoparticles with both organic antifouling and antibacterial properties. *J. Membr. Sci.* **387–388**, 1–6 (2012).
32. Nikkola, J. et al. Surface modification of thin film composite RO membrane for enhanced anti-biofouling performance. *Membr. Sci.* **444**, 192–200 (2013).
33. Adepu, S. & Khandelwal, M. Broad-spectrum antimicrobial activity of bacterial cellulose silver nanocomposites with sustained release. *J. Mater. Sci.* **53**, 1596–1609 (2018).
34. Xu, L. et al. Silver nanoparticles: synthesis, medical applications and biosafety. *Theranostics* **10**, 8996–9031 (2020).
35. Akhavan, O. & Ghaderi, E. Self-accumulated Ag nanoparticles on mesoporous TiO₂ thin film with high bactericidal activities. *Surf. Coat. Technol.* **204**, 3676–3683 (2010).
36. Carpenter, A. W., de Lannoy, C. & Wiesner, M. R. Cellulose nanomaterials in water treatment technologies. *Environ. Sci. Technol.* **49**, 5277–5287 (2015).
37. Cao, X. L., Tang, M., Liu, F., Nie, Y. & Zhao, C. Immobilization of silver nanoparticles onto sulfonated polyethersulfone membranes as antibacterial materials. *Colloids Surf. B* **81**, 555–562 (2010).
38. Park, S. et al. Immobilization of silver nanoparticle-decorated silica particles on polyamide thin film composite membranes for antibacterial properties. *J. Membr. Sci.* **499**, 80–91 (2016).
39. Rahaman, M. S. et al. Control of biofouling on reverse osmosis polyamide membranes modified with biocidal nanoparticles and antifouling polymer brushes. *J. Mater. Chem. B* **2**, 1724–1732 (2014).
40. Li, W. D. et al. Facile preparation and characteristic analysis of sulfated cellulose nanofibril via the pretreatment of sulfamic acid-glycerol based deep eutectic solvents. *Nanomaterials* **11**, 2778–2794 (2021).

ACKNOWLEDGEMENTS

This work was supported by the National Natural Science Foundation of China (Grant no. 31901267); the Provincial Key Research and Development Program of Shandong (Grant nos. 2021CXGC010601, 2019JZZY010326, and 2019JZZY010328); a Pilot Project for Integrating Science, Education and Industry (2022PY042) and a project (Grant no. ZR2019BC042) supported by Shandong Provincial Natural Science Foundation.

AUTHOR CONTRIBUTIONS

M.H.: Conceptualization, validation, formal analysis, resources, writing—original draft, writing—review & editing, supervision, funding acquisition. W.-D.L.: Methodology, validation, formal analysis, investigation, data curation, writing—original draft. J.-C.C.: Formal analysis, methodology. Z.-G.Z.: Data curation. X.-F.W.: Formal analysis, methodology. G.-H.Y.: Supervision, funding acquisition.

COMPETING INTERESTS

The authors declare no competing interests.

ADDITIONAL INFORMATION

Supplementary information The online version contains supplementary material available at <https://doi.org/10.1038/s41545-022-00217-7>.

Correspondence and requests for materials should be addressed to Ming He or Gui-Hua Yang.

Reprints and permission information is available at <http://www.nature.com/reprints>

Publisher's note Springer Nature remains neutral with regard to jurisdictional claims in published maps and institutional affiliations.



Open Access This article is licensed under a Creative Commons Attribution 4.0 International License, which permits use, sharing, adaptation, distribution and reproduction in any medium or format, as long as you give appropriate credit to the original author(s) and the source, provide a link to the Creative Commons license, and indicate if changes were made. The images or other third party material in this article are included in the article's Creative Commons license, unless indicated otherwise in a credit line to the material. If material is not included in the article's Creative Commons license and your intended use is not permitted by statutory regulation or exceeds the permitted use, you will need to obtain permission directly from the copyright holder. To view a copy of this license, visit <http://creativecommons.org/licenses/by/4.0/>.

© The Author(s) 2022